

Journal Pre-proof

Coupling Metal-Organic Framework Nanosphere and Nanobody for Boosted Photoelectrochemical Immunoassay of Human Epididymis Protein 4

Kaiyang Chen, Jiyang Xue, Qing Zhou, Yue Zhang, Mingming Zhang, Yuanjian Zhang, Hai Zhang, Yanfei Shen



PII: S0003-2670(20)30166-5

DOI: <https://doi.org/10.1016/j.aca.2020.02.011>

Reference: ACA 237443

To appear in: *Analytica Chimica Acta*

Received Date: 1 October 2019

Revised Date: 28 December 2019

Accepted Date: 6 February 2020

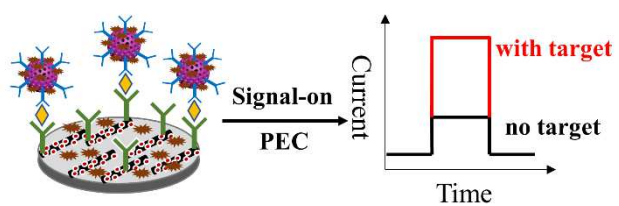
Please cite this article as: K. Chen, J. Xue, Q. Zhou, Y. Zhang, M. Zhang, Y. Zhang, H. Zhang, Y. Shen, Coupling Metal-Organic Framework Nanosphere and Nanobody for Boosted Photoelectrochemical Immunoassay of Human Epididymis Protein 4, *Analytica Chimica Acta*, <https://doi.org/10.1016/j.aca.2020.02.011>.

This is a PDF file of an article that has undergone enhancements after acceptance, such as the addition of a cover page and metadata, and formatting for readability, but it is not yet the definitive version of record. This version will undergo additional copyediting, typesetting and review before it is published in its final form, but we are providing this version to give early visibility of the article. Please note that, during the production process, errors may be discovered which could affect the content, and all legal disclaimers that apply to the journal pertain.

© 2020 Published by Elsevier B.V.

Y.F.S.(*) conceived and designed the experiments. K.Y.C. prepared and characterized the nPCN-224 nanohybrid, fabricated the immunosensor and performed the sensing experiments. J.Y.X. and H.Z.(*) prepared the Nanobodies. Q.Z., Y.Z., M.M.Z. and Y.Y.Z. contributed to the sensing data collection. All authors contributed to the analysis and discussion of the results. K.Y.C. and Y.F.S.(*) wrote the manuscript, and all authors reviewed the manuscript. K.Y.C. and J.Y.X. contributed equally. Y.F.S.(*) supervised the project.

Graphical abstract



Journal Pre-proof

Coupling Metal-Organic Framework Nanosphere and Nanobody for Boosted Photoelectrochemical Immunoassay of Human Epididymis Protein 4

Kaiyang Chen^{#1}, Jiyang Xue^{#2}, Qing Zhou¹, Yue Zhang¹, Mingming Zhang¹, Yuanjian Zhang¹, Hai Zhang^{*2} and Yanfei Shen^{*1}

¹ Medical School, School of Chemistry and Chemical Engineering, Southeast University, Nanjing 210009, China.

² Department of Pharmacy, Shanghai First Maternity and Infant Hospital, Tongji University School of Medicine, Shanghai 201204, China

[[#]] These authors contributed equally to this work.

[^{*}] Corresponding authors. Email: Yanfei.Shen@seu.edu.cn; zhxdks2005@126.com

Abstract

A “signal-on” photoelectrochemical (PEC) immunosensor for highly sensitive detection of Human Epididymis Protein 4 (HE4), a new serum biomarker of ovarian cancer with small molecular weight, was fabricated by coupling the porphyrin-based metal-organic framework (MOF) nanosphere (nPCN-224) and Nanobody (Nb). To label the Nb, the nPCN-224 with an average size of 160-200 nm was prepared by solvothermal method. The mechanism for the photocurrent generation of nPCN-224 was systematically investigated, showing that the dissolved O_2 in aqueous solution participated the charge separation and transport during the photoelectric conversion by generating $O_2^{\cdot-}$, which resulted in a 6-fold enhanced photocurrent by using ascorbic acid as the $O_2^{\cdot-}$ scavenger. Moreover, the inherent structural porosity of nPCN-224 demonstrated advantage for reactant accessibility. Due to the superior properties of nPCN-224, and the high specificity and affinity of Nbs, the immunosensor exhibited a broad detection range from $1.00 \text{ pg}\cdot\text{mL}^{-1}$ to $10.0 \text{ ng}\cdot\text{mL}^{-1}$ and a detection limit of $0.560 \text{ pg}\cdot\text{mL}^{-1}$, lower than most methods reported before. The immunosensor could clearly distinguish ovarian cancer patients in different stages from healthy individuals, and the as-obtained results matched well with those by traditional electrochemiluminescence immunoassay method from the hospital. This work would open a new avenue for PEC immunosensors in clinical diagnostics and evaluation of potential clinical efficacy.

Keywords: metal-organic framework, photoelectrochemical, immunosensor,

Human Epididymis Protein 4, Nanobody

1. Introduction

Among the common malignant tumors of female reproductive organs, ovarian cancer remains a major cause of death in gynecological malignancy of women [1]. More than 60% of patients are diagnosed at advanced stage, that is, stage III or later, with a 5-year survival rate of about 46%. However, the 5-year survival rate can be up to 92% when the diagnosis occurs at stage I. Human epididymis protein 4 (HE4) has recently emerged as a new serum biomarker of ovarian cancer with a molecular weight of approximately 25 kDa [2], which shows predominance for the early diagnosis of ovarian cancer and is impervious to the menopausal status[3-5]. Thus, developing highly sensitive and selective analytical methods with high reliability is of critical significance in the early cancer diagnosis.

Current methods for the detection of HE4 include enzyme-linked immunosorbent assay (ELISA), electrochemical immunosensor, chemiluminescent immunoassay, electrochemiluminescent immunoassay, radioimmunoassay, localized surface plasmon resonance (LSPR) biosensor, molecularly imprinting sensor, and optical assay and so on [2, 6-13]. For instance, Heller et al developed a noninvasive detection via an optical nanosensor implant [11]. Zheng et al designed an ultrasensitive electrochemical immunoassay based on Cargo release from nanosized PbS colloidosomes [14].

As an emerging bioanalytical technique, photoelectrochemical (PEC) bioanalysis,

which combines photochemistry and electrochemistry, has drawn much attention recently [15-18], since it not only equips with merits of low cost, simple instrument and high selectivity, but also shows advantages of high sensitivity and low background resulting from the separation of excitation light source and readout signal [19-21]. As one of critical factors for PEC bioanalysis, PEC active species have been extensively exploited for use, including metal-containing semiconductors such as TiO₂, ZnO, WS₂ nanosheet, CdS and carbon-nanomaterials etc. [22-29]. For instance, Li et al recently developed a “signal-off” PEC immunosensor for HE4 by using WS₂ nanosheet as probes [29]. Nevertheless, it is still essential to develop more photoactive materials with high PEC performance, features of environmental benign and easy biofunctionalization for further applications of PEC biosensing.

Metal-organic frameworks (MOFs), as an emerging class of functional materials with highly ordered porosity and large specific surface area [30-33], have been extensively applied in PEC biosensing [34, 35], offering some interesting and distinct advantages over other nanoprobables. For example, Li et al reported a novel nanocomposite IBABr-Au@Zn-MOF as both the substrate materials and probes for the construction of a “signal-off” PEC immunosensor [36]; Shan’s group reported a “signal-off” PEC sensor using a Zr-based MOF (PCN-222) as the signal probe based on the steric hindrance effect generated by the coordination interaction between Zr-O clusters and phosphate groups [37]; Ai and Liu’s group constructed photoactive materials for PEC biosensing by using MOFs as accommodation for photoactive probes such as black TiO₂ and Ru(bpy)₃²⁺ [38]. Among them, MOFs have been

usually applied as both the substrates and probes for “signal-off” biosensors due to the large size of crystalline MOFs, or as hosts for the accommodation of photoactive dyes thanks to its high porosity. However, the “signal-on” PEC biosensor using nanoscaled MOFs as photoactive element has been seldom reported [39].

Herein, by choosing carboxyl groups-functionalized porphyrin as ligands, a porphyrin-based MOF nanosphere (nPCN-224) was applied as a PEC probe for a “signal-on” PEC immunosensor for the detection of HE4 (Fig. 1). The MOFs with carboxyl groups-functionalized porphyrin as ligands are expected to show not only excellent photoelectric activity, but also a friendly biointerface for further biomolecules conjugation in biosensing. Since HE4 has a relatively small molecular size (with a molecular weight of approximately 25 kDa), the immunoassay using Nanobody (Nb, with a molecular weight of 12~15 kDa) instead of conventional monoclonal antibody (mAb) would result in a high sensitivity [40, 41]. The PEC immunosensor by using nPCN-224 as a PEC probe and Nbs as recognition units not only showed superior sensing performance so far, but also demonstrated high reliability for practical assay of HE4 level in both spiked samples and real clinical specimens. This work would open a new avenue for the future clinical diagnostics and evaluation of potential clinical efficacy.

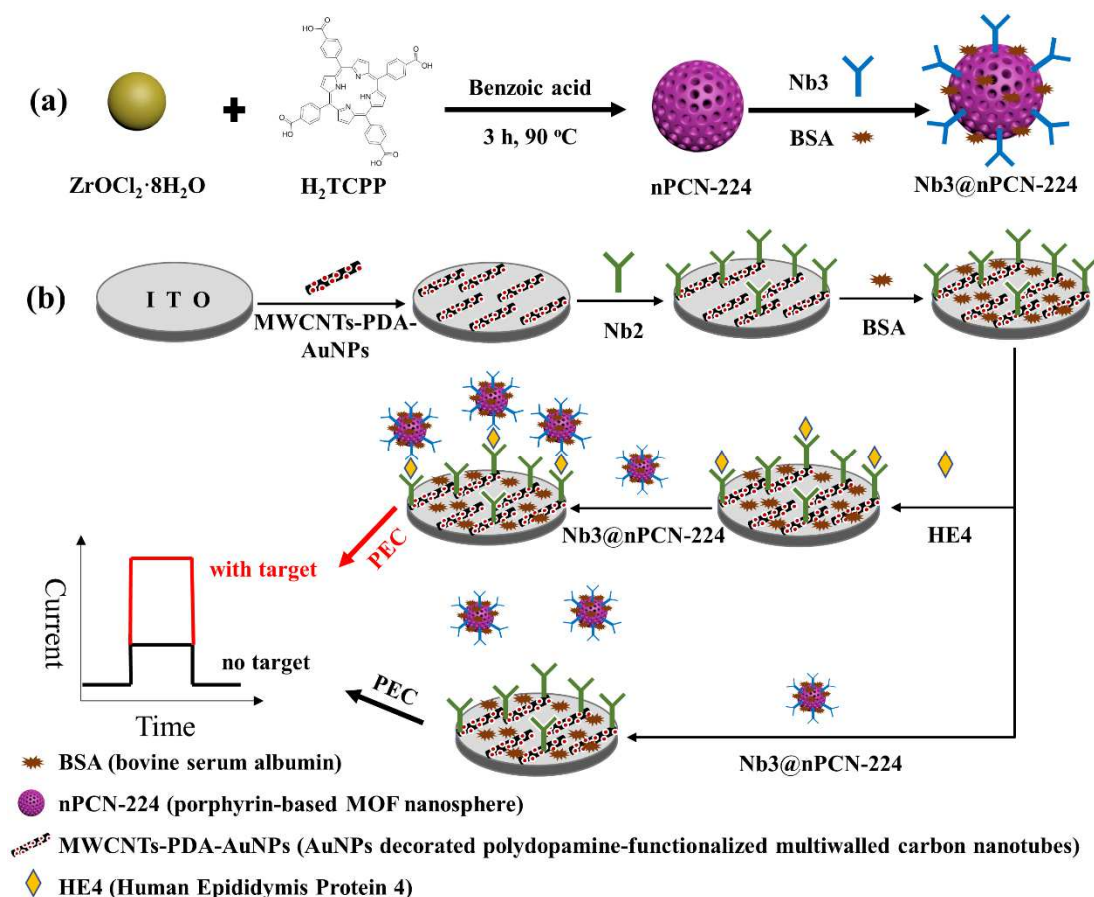


Figure 1. Scheme for the preparation of Nb3@nPCN-224 (a) and fabrication of photoelectrochemical HE4 immunosensor (b).

Experimental Section

1.1 Materials and Reagents

Meso-tetra(4-carboxyphenyl)porphyrin (H_2TCPP), zirconium(IV) oxychloride octahydrate, superoxide dismutase (SOD), chlorauric acid (HAuCl_4), BSA, 1-ethyl-3-(3-dimethylaminopropyl) carbodiimide (EDC) and N-hydroxysuccinimide (NHS) were purchased from Sigma-Aldrich (USA). Benzoic acid (BA), N,N-dimethylformamide (DMF), mannitol, acetone, ethanol, ascorbic acid (AA) and L-Cysteine (L-Cys) were obtained from Sinopharm Chemical Reagent Co., Ltd. (Shanghai, China). Dopamine (DA) was provided by J&K Chemical Co., Ltd. (USA).

Carboxyl-functionalized multiwalled carbon nanotubes (MWCNTs) and human serum albumin (HSA) were offered by Nanjing XFNANO Materials Tech Co., Ltd. (Nanjing, China) and Simmcere Co., Ltd. (Nanjing, China), respectively. Potassium ferricyanide ($K_3Fe(CN)_6$) and potassium ferrocyanide ($K_4Fe(CN)_6$) were offered by Shanghai Lingfeng Chemical Reagent Co., Ltd. (Shanghai, China). Carcinoembryonic antigen (CEA) and alpha-fetoprotein (AFP) were obtained from Beijing Key-Bio Biotech Co., Ltd. (Beijing, China). Phosphate buffer solution (PBS), Tris-HCl buffer and trisodium citrate dihydrate ($Na_3C_6H_5O_7 \cdot 2H_2O$) were purchased from Sangon Biotech (Shanghai, China). Indium tin oxides (ITO, 6.2-6.8 Ω/sq) was supplied by Zhuhai Kaivo Optoelectronic Technology Co., Ltd. (Zhuhai, China). Ultrapure water (18.2 $M\Omega \cdot cm$, Milli-Q) was used for the whole experiments.

1.2 Apparatus

Electrochemical impedance spectroscopy (EIS) were carried out on a CHI 660e workstation (Shanghai, China) using a three-electrode system. The counter electrode was a platinum wire, the reference electrode was an Ag/AgCl (saturated KCl) electrode and the modified ITO electrode was used as the working electrode. PEC studies were performed with a 150 W xenon lamp as the source of visible light (Zolix Instruments Co., Ltd., Beijing, China) at room temperature. The PEC measurements were performed in 10 mM PBS (pH = 5) containing 0.1 M AA at a constant biased potential of -0.05 V. Scanning electron microscopy (SEM) images were obtained from a Zeiss Ultra Plus (Germany). Transmission electron microscopy (TEM) images and high-resolution transmission electron microscopy (HRTEM) images were measured

by a field emission electron microscopy (JEM-2100f, JEOL, Japan) at an acceleration voltage of 200 kV (FEI, USA). Elemental analysis was recorded on the Oxford X-Max Energy Dispersive Spectroscopy (EDS) (England). UV–vis absorption spectra were recorded by a Cary100 UV–vis spectrophotometer (Agilent, USA). Powder X-ray diffraction (XRD) was detected by a SmartLab (3) X-ray diffractometer (Rigaku, Japan). Fourier transform infrared (FTIR) spectra were performed by a Nicolet iS10 FTIR spectrometer (Thermo, USA) loaded with an attenuated total reflection (ATR) setup. Fluorescence spectra were recorded by a FluoroMax-4 spectrofluorometer with the xenon discharge lamp excitation (Horiba, Japan). The dynamic light scattering (DLS) technique was used to analyze the particle size distribution by a NanoBrook Omni instrument (Brookhaven, USA). The DFT pore size distribution and Brunauer-Emmett-Teller (BET) surface area calculated from N₂ adsorption-desorption isotherms at 77 K were obtained from NovaWin 1000e (Quantachrome, USA).

1.3 Synthesis of MWCNTs-PDA-AuNPs

MWCNTs-PDA-AuNPs was synthesized based on a previous report with a slight modification [42]. Firstly, 10 mg of carboxyl-functionalized MWCNTs were dispersed in 0.01 M Tris-HCl buffer (pH = 8.5), and followed by sonicating for 10 min. Then, the precipitate was re-dispersed in Tris-HCl buffer (pH = 8.5) containing 2 mg·mL⁻¹ DA after centrifugation and washing with Tris-HCl buffer, and then stirred for 24 h at the room temperature. Next, the MWCNTs-PDA was collected by centrifugation and

washing with ultrapure water. Afterwards, 70 μL of 0.1 M HAuCl_4 aqueous solution was added to MWCNTs-PDA dispersion, and subsequently 1 mL of 0.1 M sodium citrate was added to the above solution drop by drop under stirring. After stirring for 2 h at room temperature, the MWCNTs-PDA-AuNPs nanohybrids were obtained by centrifugation and washing with ultrapure water.

1.4 Synthesis of nPCN-224 and Nb₃@nPCN-224

The nPCN-224 was synthesized according to a previous literature with minor modifications [43]. H_2TCPP (10 mg, 0.13 mmol), $\text{ZrOCl}_2 \cdot 8\text{H}_2\text{O}$ (30 mg, 0.93 mmol) and BA (290 mg, 24 mmol) were dissolved in DMF (10 mL) in a 50 mL Teflon-lined autoclave and the resulting solution was heated at 90 °C for 3 h in an oven. After cooling to room temperature, purple crystals were obtained by centrifugation and washing with DMF for several times. The obtained nPCN-224 was resuspended in DMF for further use. To further combine with the labeled Nb (Nb₃), 1 mg of nPCN-224 dissolved in DMF was washed with ethanol again firstly. Then, the obtained nPCN-224 were re-dispersed in 1.0 mL of 10 mM PBS solution, and followed by sonicating for 10 min. Next, the resulting suspension was added into the freshly prepared 1.0 mL of 10 mM PBS solution containing 10 $\text{mg} \cdot \text{mL}^{-1}$ NHS and 20 $\text{mg} \cdot \text{mL}^{-1}$ EDC under stirring for 2 h at room temperature under darkness. After centrifugation and washing with 10 mM PBS solution, the precipitate was resuspended in 2.2 mL of 10 mM PBS solution containing 20 μg Nb₃ and the suspension was stirred at 4 °C for 12 h under darkness. Afterwards, the precipitate was collected by centrifugation and added into 2.0 mL of 10 mM PBS solution containing

20 mg BSA with extra stirring at 37 °C for 1 h. Finally, the obtained Nb3@nPCN-224 was stored at 4 °C under darkness before use.

1.5 Fabrication of Photoelectrochemical Immunosensor

Before the surface modification, ITO electrodes were cleaned ultrasonically with acetone, ethanol and ultrapure water in sequence for 15 min and then were dried under N₂ flow. Next, 10 μL of the obtained MWCNTs-PDA-AuNPs dispersion (0.75 mg·mL⁻¹) was drop-casted onto the ITO electrode (0.4 × 0.4 cm²) and dried at 37 °C in an electro-heating standing-temperature cultivator for 5 h. Afterwards, 10 μL of EDC/NHS solution (10 mg·mL⁻¹/20 mg·mL⁻¹) as activating agent was drop-casted onto the electrode and kept at room temperature for 2 h. Then, the unreacted activation agent was washed away by 10 mM PBS solution, and 10 μL of the capture Nb (Nb2, 10 μg·mL⁻¹) in 10 mM PBS was dropped onto the surface of the electrode at 4 °C for 12 h. After rinsing with 10 mM PBS solution, 10 μL of BSA (1% w/v) in 10 mM PBS was added dropwise onto the Nb2 modified ITO electrode at 37 °C for 30 min to block the non-specific sites. After that, 10 μL of HE4 antigen with various concentrations was further dropped onto the modified ITO electrode, and incubated at 37 °C for 60 min. Followed by rinsing with 10 mM PBS solution, 10 μL of Nb3@nPCN-224 dispersion was dropped onto the above ITO electrode and incubated at 37 °C for 60 min. At last, the HE4 immunosensor was successfully constructed after rinsing with 10 mM PBS solution.

1.6 Detection of HE4 in Spiked Samples and Real Clinical Specimens

The serum from healthy people was diluted 100 times using 10 mM PBS solution.

Then the target HE4 was added into the spiked serum samples resulting in 10.0, 0.100 and 1.00×10^{-3} ng·mL⁻¹ HE4, respectively, which were analyzed by the as-fabricated PEC immunosensor. Furthermore, the immunosensor was also applied for the detection of HE4 level in the clinical specimens from non-ovarian cancer patients and ovarian cancer patients, all of which were collected from Zhongda hospital. For each sample, there were three independently repeated measurements, and the concentration of HE4 in these samples was calculated based on the calibration curve. For comparison, the detection results were compared with those obtained by electrochemiluminescence immunoassay (ECLIA) from Zhongda hospital.

2. Results and Discussion

2.1 Characterization of MWCNTs-PDA-AuNPs Nanohybrids.

In order to enhance the performance of the PEC immunosensor, MWCNTs-PDA-AuNPs nanohybrids showing high conductivity and stability were chosen as the substrate material to modify the ITO electrodes and link the capture antibody Nb2 [42, 44, 45]. The successful preparation of MWCNTs-PDA-AuNPs nanohybrids were firstly manifested by TEM. As shown in Fig. 2A, MWCNTs exhibited a tubular morphology, and the diameter of MWCNTs-PDA (Fig. 2B) was much wider than that of MWCNTs (Fig. 2A), which indicated that PDA was successfully coated onto the surface of MWCNTs. After the treatment with HAuCl₄, the AuNPs with a diameter of ca. 6 nm were homogeneously anchored on the surface of MWCNTs-PDA (Fig. 2C, D). The successful synthesis of MWCNTs-PDA-AuNPs

was also confirmed by UV-vis spectra. As shown in Fig. S3, both the MWCNTs and MWCNTs-PDA showed a broad absorption peak in the whole UV-vis region. While after the modification of AuNPs, an obvious absorption peak around 530 nm was observed, which was attributed to the characteristic absorption of AuNPs. All the above results demonstrated that the MWCNTs-PDA-AuNPs nanohybrids were successfully synthesized, which would be applied as a substrate for the further conjugation of biomolecules, e.g., Nb2.

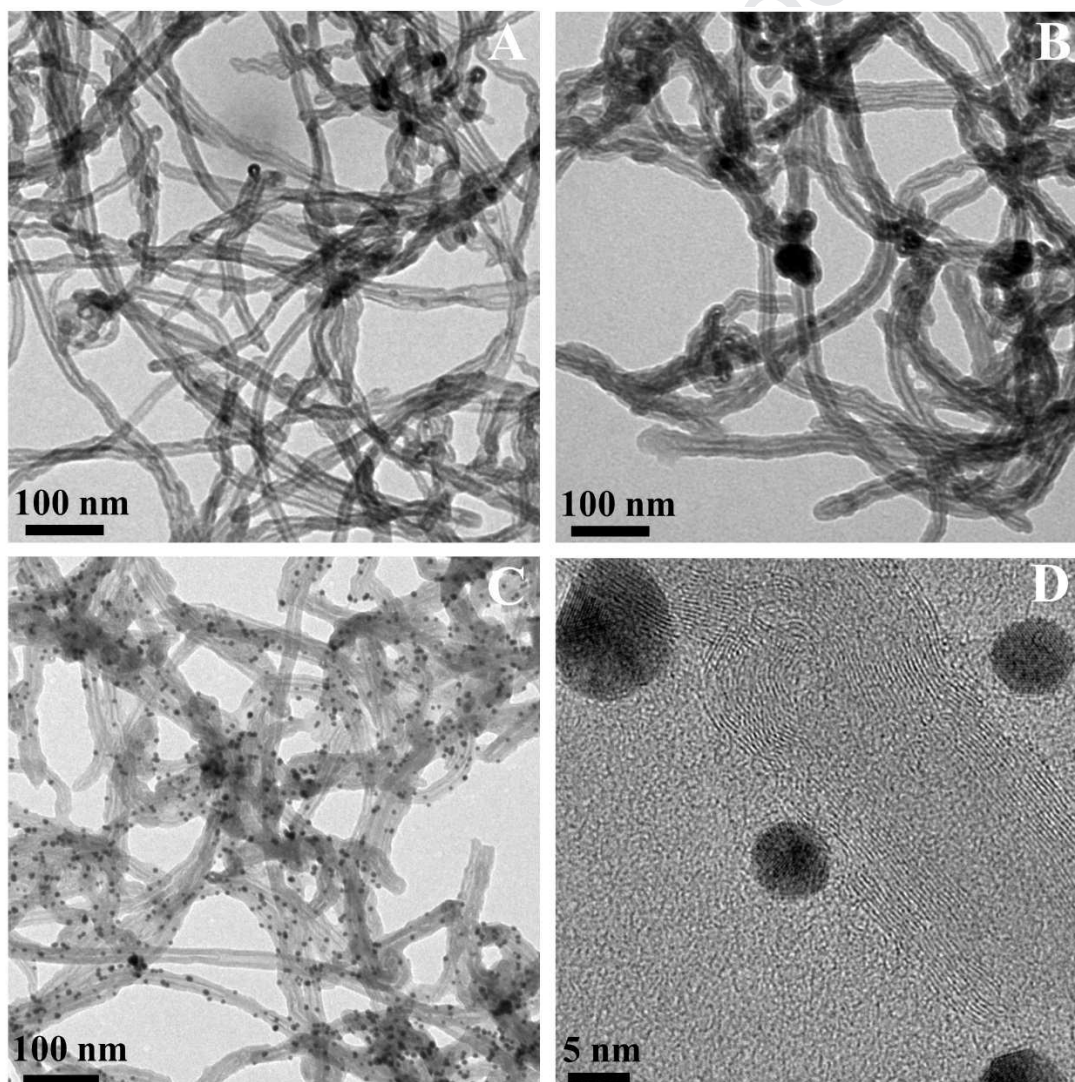


Figure 2. TEM images of MWCNTs (A), MWCNTs-PDA (B) and

MWCNTs-PDA-AuNPs (C), and the HRTEM image of MWCNTs-PDA-AuNPs (D).

2.2 Characterization of nPCN-224.

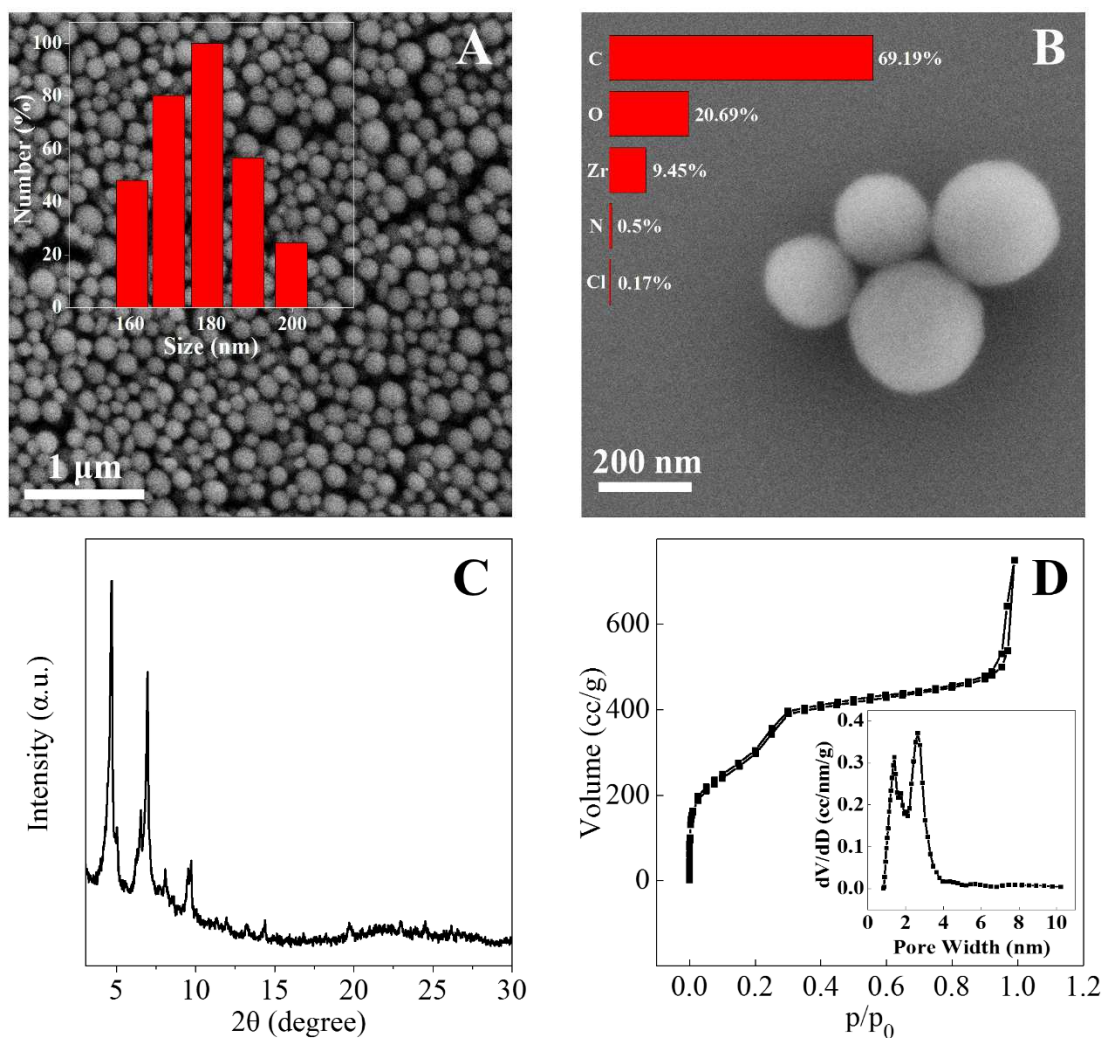


Figure 3. SEM images of nPCN-224 (A, B). The inset in (A) is the DLS size distribution histogram of nPCN-224. The inset in (B) is the elemental atomic percentage by EDS in nPCN-224. XRD spectrum (C) and Nitrogen adsorption-desorption (D) of nPCN-224. The inset in (D) is the pore size distribution at 77 K with N_2 .

PCN-224, a porphyrin-based Zr_6 MOF, showed excellent stability, good biocompatibility and superior optical properties [46-48]. To obtain PCN-224 nanosphere (nPCN-224), a diluted ligand solution was used for the synthesis compared with that for the single crystalline PCN-224 [43]. The morphology of the nPCN-224 obtained was investigated by SEM (Fig. 3A, B). The SEM images showed that the nPCN-224 exhibited a spherical morphology, with the particle size in range of 160 nm~200 nm, as confirmed by DLS analysis (Fig. 3A, inset). Furthermore, EDS analysis (Fig. 3B, inset) showed that the chemical composition of the as-obtained complex was consistent with that of PCN-224. In addition, the XRD result of the nPCN-224 (Fig. 3C) showed that the main diffraction peaks were at 4.68° , 6.96° , 8.08° and 9.70° , which were consistent with those of the single crystalline PCN-224 [43]. Meanwhile, the porosity of the as-synthesized nPCN-224 was investigated by N_2 adsorption-desorption measurements. As shown in Fig. 3D, the BET surface area and pore volume of nPCN-224 were calculated to be $1137\text{ m}^2\cdot\text{g}^{-1}$ and $0.873\text{ cm}^3\cdot\text{g}^{-1}$ with two pore sizes at around 1.3 nm and 2.7 nm, respectively. The large surface area and high porosity of nPCN-224 would be highly desirable for improving the loading of antibody and promoting the electron transfer to enhance the sensitivity of the followed PEC immunosensor. Moreover, the inherent structural porosity of nPCN-224 demonstrated advantage for reactant accessibility, which would be beneficial for enhancing the separation of photogenerated electrons and holes.

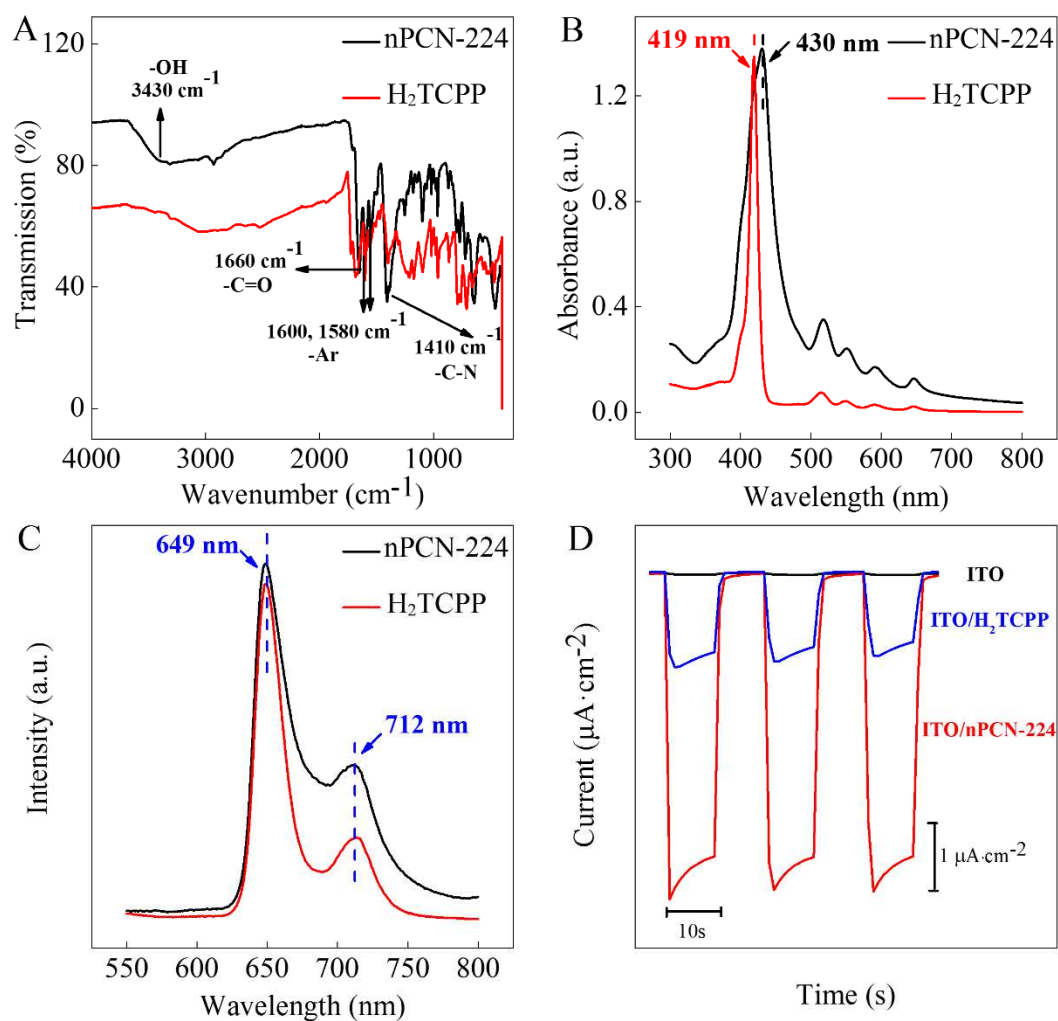


Figure 4. FT-IR (A), UV-vis (B) and PL emission ($\lambda_{\text{ex}} = 420$ nm) (C) spectra of nPCN-224 and H₂TCPP in DMF. (D) Photocurrent responses of ITO, ITO/H₂TCPP and ITO/nPCN-224 in 10 mM phosphate buffer solution (PBS) (pH=5) with 0.1 M AA.

The spectroscopic properties of the nPCN-224 were also investigated. As shown in Fig. 4A, the FTIR spectra revealed some characteristic functional groups of nPCN-224 such as -C-N (1410 cm^{-1}), -Ar (1600 and 1580 cm^{-1}), -C=O (1660 cm^{-1}) and -OH (3430 cm^{-1}), which were consistent with those of H₂TCPP. Meanwhile, the

UV-vis spectra (Fig. 4B) showed that the maximum Soret absorption of nPCN-224 (430 nm) in DMF was red-shifted by 11 nm compared with that of free H₂TCPP (419 nm), which could be attributed to the hydrophobic cavity of nPCN-224 whose Soret band is easily shifted by changing the solvent with different dielectric constants [49]. Moreover, the nPCN-224 exhibited a strong emission peak at 649 nm with a shoulder peak at 712 nm under the excitation at 420 nm (Fig. 4C), which was matched with the emission peak of H₂TCPP. Thus, the as-synthesized nPCN-224 retained most of the optical properties of H₂TCPP, which provided the possibility for nPCN-224 to be as a PEC probe. To assess the photoelectric activities of the nPCN-224, a standard PEC cell was fabricated for measuring the photocurrent generation with chopped light irradiation. As shown in Fig. 4D, the photocurrent was prompt, steady, and reproducible. More importantly, with the same coating amount, the ITO/nPCN-224 showed a 3.5 times higher photocurrent than that of its precursor, H₂TCPP, demonstrating the important role of the porous structure of the nPCN-224. On one hand, the highly porous structure and the high surface area were beneficial for the electron transfer; on the other hand, the highly porous structure was in favor of enriching the small molecules such as the scavenger AA in the solution, which was expected to promote the separation of photogenerated electrons and holes[37]. Therefore, the nPCN-224 was selected as a PEC probe for the construction of PEC immunosensor in the following study.

2.3 Mechanism for the Photocurrent Generation.

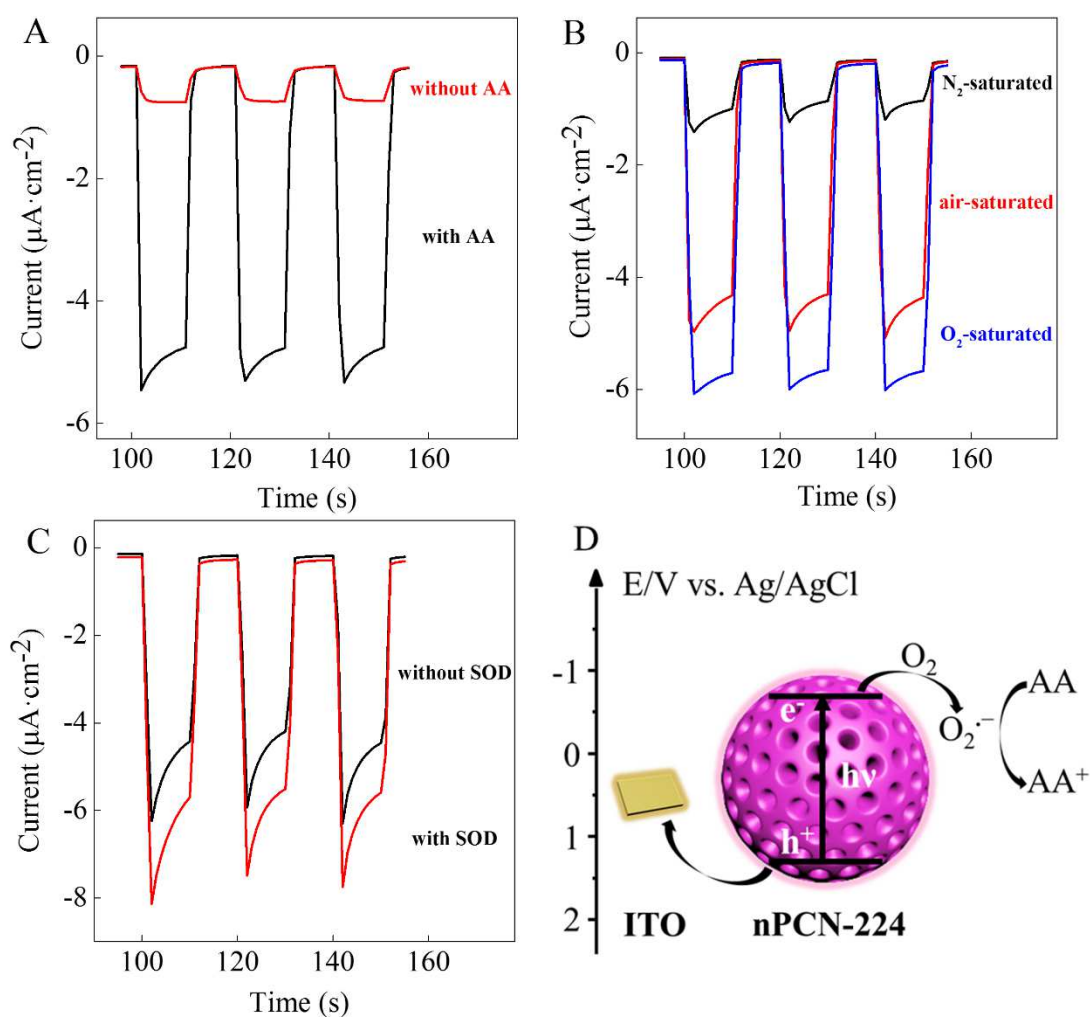


Figure 5. (A) Photocurrent responses of ITO/nPCN-224 in 10 mM PBS (pH=5) with 0.1 M AA and without AA. (B) Photocurrent responses of ITO/nPCN-224 in 10 mM PBS (pH=5) with 0.1 M AA in the case of the N_2 -saturated, the air-saturated and the O_2 -saturated. (C) Photocurrent responses of ITO/nPCN-224 in 10 mM PBS (pH=5) containing 0.1 M AA with and without 0.01 $\text{mg} \cdot \text{mL}^{-1}$ superoxide dismutase (SOD).

(D) The mechanism of photocurrent generation with ITO/nPCN-224.

The mechanism for the photocurrent generation of nPCN-224 was systematically investigated. As shown in Fig.5B, the photocurrent of ITO/nPCN-224 in the air-saturated solution was much higher than that in the N₂-degassed solution, and the photocurrent was further enhanced in the O₂-saturated solution, indicating that the dissolved O₂ in aqueous solution participated in the charge separation and transport during the photoelectric conversion. To further explore the photoelectric conversion process, AA, a typical O₂^{•-} scavenger was added to the solution. As shown in Fig. 5A, the photocurrent of ITO/nPCN-224 in the electrolyte with AA was about 6 times higher than that without AA, suggesting that AA might be applied as an O₂^{•-} scavenger, which promoted the separation of photogenerated electrons and holes and resulted in the enhancement of photocurrent. To further confirm the intermediate product during the PEC process, the possible reactive species including superoxide anion (O₂^{•-}) and hydroxyl radicals (·OH) were probed with selective depletion agents, superoxide dismutase (SOD) and mannitol [50], respectively. The photocurrent with SOD was higher than that without SOD, which could be contributed to the depletion of O₂^{•-} (Fig. 5C). Furthermore, the photocurrent was dropped after adding mannitol to the electrolyte (Fig. S4), which further suggested that the O₂^{•-} was generated during the process of photoelectric conversion. Meanwhile, it should be noted that the photocurrent only increased a little with the addition of SOD, which could be attributed to the comparable oxidation capacity of AA and SOD [51]. Thereafter, the

mechanism of the photocurrent generation of nPCN-224 was proposed as shown in Fig. 5D. Irradiated by light, the nPCN-224 absorbed photons, and the excited electrons transferred from the valence band to the conduction band, leaving holes in the valence band. Then, dissolved oxygen in the electrolyte solution accepted electrons from the conduction band, producing $O_2^{\cdot-}$, which was eliminated by AA. Meanwhile, the excited holes were consumed by electrons from the ITO. Thus, the presence of AA and dissolved oxygen effectively suppressed the recombination of electro-hole pairs, resulting in high photoelectric conversion efficiency of nPCN-224, which was in favor of enhancing the sensing performance of the PEC biosensor by using nPCN-224 as a PEC probe.

2.4 Fabrication of the Immunosensor and Detection of Target HE4.

Our previous report displayed that by using Nb that has a small molecular weight (12~15 kDa) and unique physiochemical properties, the direct immunoassay can be applied for detection of the small molecule instead of the traditional competitive immunoassay with complicated procedure by using monoclonal antibody (mAb). Noticed the small molecular size (with a molecular weight of approximately 25 kDa) of HE4, two Nbs, Nb2 and Nb3 were screened out and purified as recognition units for the fabrication of PEC immunosensor for HE4 (see Fig.S1 and Fig.S2, and more discussion in Supporting Information) The construction process was confirmed by photocurrent measurements with chopped light irradiation by a standard PEC cell. As shown in Fig. 6A, after the electrode was modified with the MWCNTs-PDA-AuNPs nanohybrids, the photocurrent was enhanced obviously compared with that of the bare ITO, which

could be attributed to the photoelectric activity of MWCNTs. After further assembly with Nb2 and HE4, the photocurrent decreased gradually, probably owing to the steric resistance and poor conductivity of these biomolecules. However, the photocurrent was significantly improved after the immunoreaction of Nb3@nPCN-224 with HE4, which indicated that the nPCN-224 labeled on Nb3 could be utilized as a “signal-on” PEC probe for the HE4 sensor. Since the nPCN-224 could be quantitatively captured onto the photoelectrode via the immunoreaction of Nb3@nPCN-224 and HE4 (Fig. 1), the amount of HE4 would be quantitatively detected by measuring the photocurrent response upon the capture of Nb3@nPCN-224. Meanwhile, the EIS measurements also confirmed the successful assembly of the immunosensor (Fig. S5). Under the optimum detection conditions (see results in Fig. S6), the photocurrent gradually increased with the amount of HE4, and the calibration curve exhibited a good linear relationship between the increased photocurrent and the logarithmic values of HE4 concentrations ranging from 1.00 pg·mL⁻¹ to 10.0 ng·mL⁻¹ (Fig. 6B). The relationship between $\Delta I/I_0$ and C_{HE4} could be expressed as $\Delta I/I_0 = 0.1714 \log C_{HE4} (\text{g}\cdot\text{mL}^{-1}) + 2.5149$ with a correlation coefficient of 0.996, and the limit of detection (LOD, $3\sigma/S$) was calculated to be 0.560 pg·mL⁻¹. Thus, the HE4 could be quantitatively detected by the proposed PEC immunosensor. Compared with other methods for HE4 assay in previous reports (Table 1), the PEC immunosensor constructed in this work exhibited superior sensing performance, thanks to the outstanding PEC performance of nPCN-224.

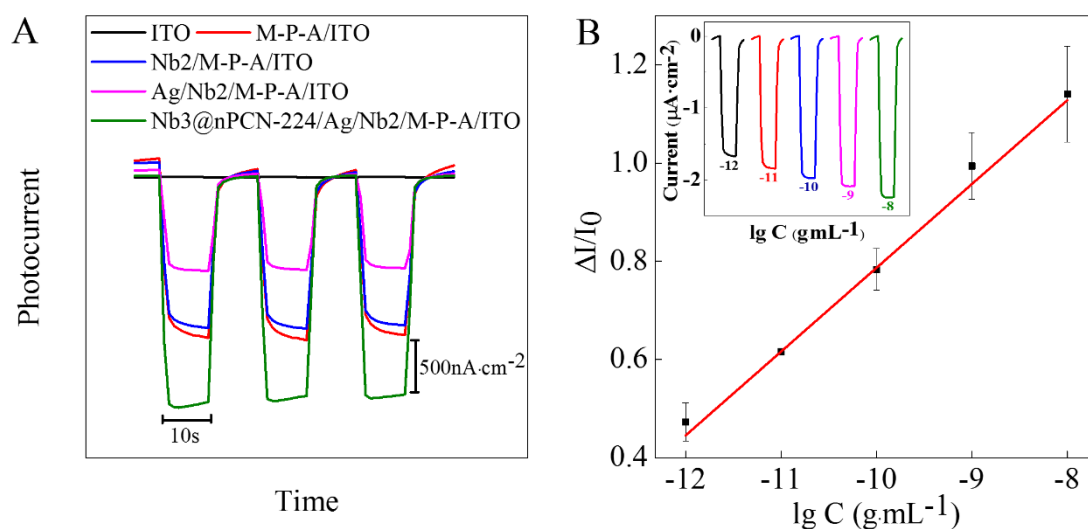


Figure 6. (A) Photocurrent responses of the HE4 immunosensor in each step during the fabrication process in 10 mM PBS solution (pH=5) containing 0.1 M AA. (B) Calibration plot of the PEC immunoassay for the detection of different concentrations of HE4 from 1.00 pg·mL⁻¹ to 10.0 ng·mL⁻¹. Inset: photocurrent responses of the PEC immunosensor to different concentrations of target HE4 antigen at 10 ng·mL⁻¹, 1.00 ng·mL⁻¹, 0.100 ng·mL⁻¹, 0.0100 ng·mL⁻¹ and 1.00 pg·mL⁻¹.

Table 1. Comparison of Different Methods for HE4 Detection.

Methods	Linear range (ng·mL ⁻¹)	LOD (ng·mL ⁻¹)	References
ELISA	0.375 ~ 22.5	0.375	[52]
Electrochemical immunosensor	1.00 ~ 100	0.200	[9]
Chemiluminescent immunoassay	0.500 ~ 37.5	4.50×10^{-3}	[10]
ECL immunosensor	1.00×10^{-5} ~ 100	3.30×10^{-6}	[53]
LSPR biosensor	0.250 ~ 250	0.100	[13]
photoelectrochemical sensor	0.0250 ~ 4.00	0.0154	[2]
photoelectrochemical immunosensor	1.00×10^{-3} ~ 10.0	5.60×10^{-4}	This work

2.5 Specificity, Reproducibility and Stability of PEC Immunosensor.

To investigate the specificity of the PEC immunosensor, the modified electrode (BSA/Nb₂/M-P-A/ITO) was incubated with some potential interferents including CEA, AFP, L-Cys, HAS and the mixture, whose concentrations were 100-fold of the HE4. As shown in Fig. 7A, the photocurrent response of the immunosensor to CEA, AFP, L-Cys and HSA was much lower than that of the HE4 and the mixture, demonstrating that the fabricated immunosensor had good selectivity for HE4. In addition, the reproducibility was investigated by fabricating five independent PEC immunosensors in the presence of 0.0100 ng·mL⁻¹ HE4. The results showed that the

relative standard deviation (RSD) was 1.54% (Fig. S7), demonstrating the proposed immunosensor had good reproducibility. As shown in Fig. 7B, the photocurrent of the proposed immunosensor still kept stable under continuous on/off irradiation cycles for 300 s. As shown in Fig. S8, there is no significant difference for the surface structures of fabricated immunosensors before and after the PEC measurements. Moreover, the photocurrent response retained 93.1%, 84.0%, 83.3% and 81.6% of the initial signal after the prepared immunosensor for $10.0 \text{ ng}\cdot\text{mL}^{-1}$ HE4 was stored at $4 \text{ }^\circ\text{C}$ under darkness for 3, 5, 7 and 14 days, respectively (Fig. 7C), further indicating that the proposed immunosensor possessed good stability.

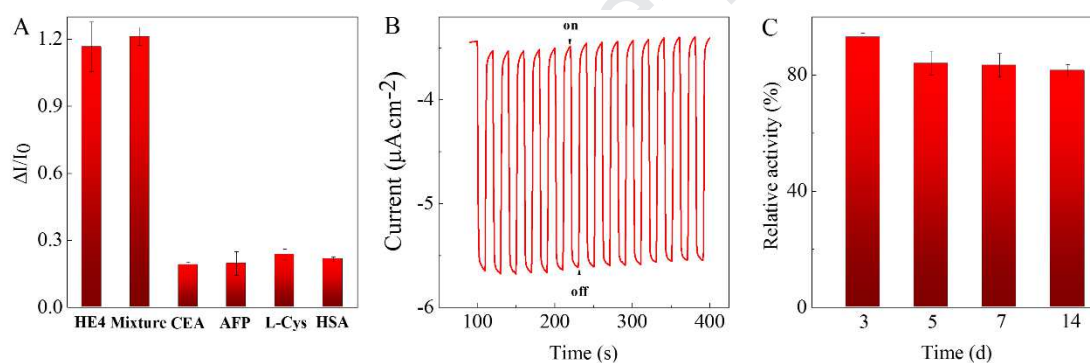


Figure 7. (A) Photocurrent responses of the proposed immunosensor for $10.0 \text{ ng}\cdot\text{mL}^{-1}$ HE4 compared to those for $1.00 \text{ }\mu\text{g}\cdot\text{mL}^{-1}$ interferents (CEA, AFP, L-Cys, HSA) and the mixture of them in 10 mM PBS solution. (B) Stability of the proposed immunosensor incubated with $10.0 \text{ ng}\cdot\text{mL}^{-1}$ HE4 under continuous on/off irradiation cycles for 300 s. (C) Stability of the proposed immunosensor for $10.0 \text{ ng}\cdot\text{mL}^{-1}$ HE4 after a storage of 3, 5, 7 and 14 days.

2.6 Preliminary Analysis of Spiked Samples and Real Clinical Specimens.

To further assess the reliability of the prepared PEC immunosensor, the recovery

experiment was carried out by analyzing the spiked samples in human serum with three different concentrations ($10.0 \text{ ng}\cdot\text{mL}^{-1}$, $0.100 \text{ ng}\cdot\text{mL}^{-1}$ and $1.00 \text{ pg}\cdot\text{mL}^{-1}$). Table 2 showed good recoveries from 90.5% to 98.6% with a relative standard deviation (RSD) less than 3.53%, which indicated that the nPCN-224-based PEC immunosensor had good reliability for HE4 detection.

Table 2. Recovery Tests of HE4 in Human Serum Samples.

Samples	Added ($\text{ng}\cdot\text{mL}^{-1}$)	Found ($\text{ng}\cdot\text{mL}^{-1}$)	RSD (%)	Recovery (%)
1	10.0	9.86	2.12	98.6
2	1.00×10^{-1}	9.41×10^{-2}	3.53	94.1
3	1.00×10^{-3}	9.05×10^{-4}	1.34	90.5

The proposed HE4 PEC immunosensor was further employed to detect the HE4 level in the serum from both healthy people and ovarian cancer patients. As shown in Fig. 8, there was an evident difference in HE4 concentration between the positive and negative groups, which indicated that the proposed HE4 immunosensor could well distinguish ovarian cancer patients in different stages from healthy individuals. It should be noted that the results detected by the PEC immunosensor matched well with the HE4 concentrations obtained by traditional electrochemiluminescence immunoassay (ECLIA) from Zhongda hospital (Table 3) and it was proved that there was no significant difference between them through Student's F and t static tests, further showing that the proposed method exhibited excellent reliability for detecting

HE4. Therefore, the nPCN-224 acting as an outstanding PEC probe made it possible for HE4 detection in clinical diagnosis. Further efforts on simplifying the operation and shortening the diagnosis time are necessary for the commercialization of the detection system.

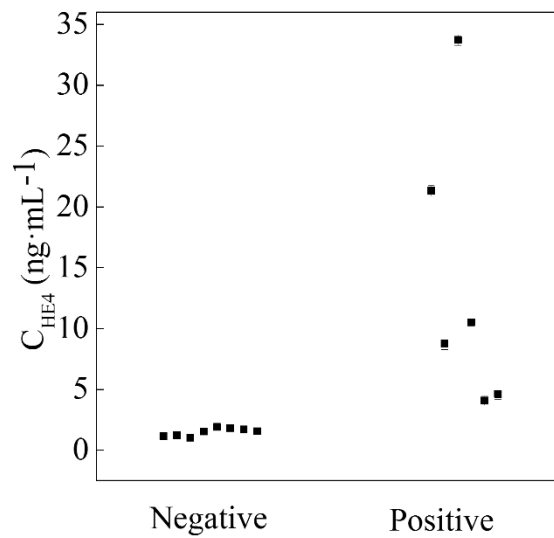


Figure 8. Photocurrent responses of the proposed PEC immunosensor for real clinical specimens from healthy people and OC patients. (The HE4 concentrations were calculated by the standard curve)

Table 3. Comparison of the Proposed PEC Immunosensor and ECLIA in Detecting HE4.

Diagnostic results	Samples	ECLIA ^a (ng·mL ⁻¹)	This work (ng·mL ⁻¹)	RSD (%)	Recovery (%)
Positive	1	22.6	21.3	2.07	94.2
	2	9.37	8.75	5.44	93.4
	3	33.1	33.7	1.30	102
	4	10.2	10.5	2.86	103
	5	3.80	4.07	8.70	107
	6	4.15	4.62	9.62	111
Negative	7	1.11	1.15	3.91	104
	8	1.20	1.21	1.72	101
	9	1.03	1.04	3.65	101
	10	1.40	1.53	7.15	109
	11	2.12	1.90	9.69	89.6
	12	1.81	1.81	6.37	100
	13	1.63	1.71	6.01	105
	14	1.63	1.57	5.58	96.3

a: The ECLIA (electrochemiluminescence immunoassay) results were obtained from Zhongda Hospital.

3. Conclusion

In summary, a porphyrin-based MOF nanosphere, nPCN-224 was successfully prepared and applied as a PEC probe to construct a “signal-on” immunosensor for detecting HE4 by using Nbs as recognition units. The nPCN-224 not only maintained many advantages of the ligand H₂TCP for photoelectric conversion, but also

exhibited advantages for reactants accessibility, thanks to the high porosity and surface area of the MOFs. The high photoelectric conversion efficiency and highly porous characteristic of nPCN-224, and the high specificity and affinity of Nbs make them attractive candidates for immunosensor applications. As a proof-of-concept, the nPCN-224 and Nbs based PEC immunosensor for HE4 detection exhibited superior performances with respect to other methods so far. A practical assay for detecting HE4 level in both spiked samples and real clinical specimens demonstrated that the proposed immunosensor could be an accessible option for highly sensitive assay. This work will pave the avenue for the future clinical diagnostics and evaluation of potential clinical efficacy.

Conflicts of interest

The authors declare no competing financial interest.

Acknowledgements

This work is supported by the National Natural Science Foundation of China (21675022, 21775018 and 81703420), Program from the Natural Science Foundation of Jiangsu Province (BK20170084 and BK20160028) and the Fundamental Research Funds for the Central Universities (2242019K3DN04 and 2242019K41036).

Appendix A. Supporting information

Supplementary data associated with this article can be found in the online version.

Author Contributions

Y.F.S. conceived and designed the experiments. K.Y.C. prepared and characterized the nPCN-224 nanohybrid, fabricated the immunosensor and performed the sensing experiments. J.Y.X. and H.Z. prepared the Nanobodies. Q.Z., Y.Z., M.M.Z. and Y.Y.Z. contributed to the sensing data collection. All authors contributed to the analysis and discussion of the results. K.Y.C. and Y.F.S. wrote the manuscript, and all authors reviewed the manuscript. K.Y.C. and J.Y.X. contributed equally. Y.F.S. supervised the project.

References

- [1] D. Holmes, OVARIAN CANCER: BEYOND RESISTANCE, *Nature* 527(7579) (2015) S217-S217.
- [2] C. Wang, X. Ye, Z. Wang, T. Wu, Y. Wang, C. Li, Molecularly Imprinted Photo-electrochemical Sensor for Human Epididymis Protein 4 Based on Polymerized Ionic Liquid Hydrogel and Gold Nanoparticle/ZnCdHgSe Quantum Dots Composite Film, *Anal. Chem.* 89(22) (2017) 12391-12398.
- [3] T. Klein, W. Wang, L. Yu, K. Wu, K.L.M. Boylan, R.I. Vogel, A.P.N. Skubitz, J.P. Wang, Development of a multiplexed giant magnetoresistive biosensor array prototype to quantify ovarian cancer biomarkers, *Biosens. Bioelectron.* 126 (2019) 301-307.
- [4] E. Anastasi, G.G. Marchei, V. Viggiani, G. Gennarini, L. Frati, M.G. Reale, HE4: a new potential early biomarker for the recurrence of ovarian cancer, *Tumour Biol.* 31(2) (2010) 113-9.
- [5] I. Hellstrom, J. Raycraft, M. Hayden-Ledbetter, J.A. Ledbetter, M. Schummer, M.

McIntosh, C. Drescher, N. Urban, K.E. Hellstrom, The HE4 (WFDC2) protein is a biomarker for ovarian carcinoma, *Cancer Res.* 63(13) (2003) 3695-3700.

[6] D. Fang, M. Pan, H. Yi, H. Dai, Z. Hong, X. Zheng, Y. Lin, Enhanced electrochemiluminescence of luminol-DBAE system based on self-assembled mesocrystalline hybrid for the detection of ovarian cancer marker, *Sens. Actuators B* 286 (2019) 608-615.

[7] D.D. Fang, S.P. Zhang, H. Dai, Y.Y. Lin, An ultrasensitive ratiometric electrochemiluminescence immunosensor combining photothermal amplification for ovarian cancer marker detection, *Biosens. Bioelectron.* 146 (2019) 7.

[8] L. Lu, B. Liu, Z. Zhao, C. Ma, P. Luo, C. Liu, G. Xie, Ultrasensitive electrochemical immunosensor for HE4 based on rolling circle amplification, *Biosens. Bioelectron.* 33(1) (2012) 216-21.

[9] Z. Qiao, H. Zhang, Y. Zhou, J. Zheng, C₆₀ Mediated Ion Pair Interaction for Label-Free Electrochemical Immunosensing with Nanoporous Anodic Alumina Nanochannels, *Anal. Chem.* 91(8) (2019) 5125-5132.

[10] G. Ruggeri, E. Bandiera, L. Zanotti, S. Belloli, A. Ravaggi, C. Romani, E. Bignotti, R.A. Tassi, G. Tognon, C. Galli, L. Caimi, S. Pecorelli, HE4 and epithelial ovarian cancer: Comparison and clinical evaluation of two immunoassays and a combination algorithm, *Clin. Chim. Acta* 412(15-16) (2011) 1447-1453.

[11] R.M. Williams, C. Lee, T.V. Galassi, J.D. Harvey, R. Leicher, M. Sirenko, M.A. Dorso, J. Shah, N. Olvera, F. Dao, D.A. Levine, D.A. Heller, Noninvasive ovarian cancer biomarker detection via an optical nanosensor implant, *Science Advances* 4(4) (2018).

[12] Q. Yan, L. Cao, H. Dong, Z. Tan, Y. Hu, Q. Liu, H. Liu, P. Zhao, L. Chen, Y. Liu, Y. Li, Y. Dong, Label-free immunosensors based on a novel multi-amplification signal strategy of TiO₂-NGO/Au@Pd hetero-nanostructures, *Biosens. Bioelectron.* 127 (2019) 174-180.

[13] J. Yuan, R. Duan, H. Yang, X. Luo, M. Xi, Detection of serum human epididymis secretory protein 4 in patients with ovarian cancer using a label-free biosensor based

- on localized surface plasmon resonance, *Int. J. Nanomed.* 7 (2012) 2921-8.
- [14] X.J. Han, H.F. Zhang, J.B. Zheng, Ultrasensitive Electrochemical Immunoassay Based on Cargo Release from Nanosized PbS Colloidosomes, *Anal. Chem.* 91(3) (2019) 2224-2230.
- [15] J. Shu, Z. Qiu, Z. Lin, G. Cai, H. Yang, D. Tang, Semiautomated Support Photoelectrochemical Immunosensing Platform for Portable and High-Throughput Immunoassay Based on Au Nanocrystal Decorated Specific Crystal Facets BiVO₄ Photoanode, *Anal. Chem.* 88(24) (2016) 12539-12546.
- [16] R. Yang, K. Zou, Y. Li, L. Meng, X. Zhang, J. Chen, Co₃O₄-Au Polyhedra: A Multifunctional Signal Amplifier for Sensitive Photoelectrochemical Assay, *Anal. Chem.* 90(15) (2018) 9480-9486.
- [17] L. Ge, Y. Xu, L. Ding, F. You, Q. Liu, K. Wang, Perovskite-type BiFeO₃/ultrathin graphite-like carbon nitride nanosheets p-n heterojunction: Boosted visible-light-driven photoelectrochemical activity for fabricating ampicillin aptasensor, *Biosens. Bioelectron.* 124-125 (2019) 33-39.
- [18] H.J. Xue, K.Y. Chen, Q. Zhou, D. Pan, Y.J. Zhang, Y.F. Shen, Antimony selenide/graphene oxide composite for sensitive photoelectrochemical detection of DNA methyltransferase activity, *J. Mater. Chem. B* 7(43) (2019) 6789-6795.
- [19] W.W. Zhao, J.J. Xu, H.Y. Chen, Photoelectrochemical bioanalysis: the state of the art, *Chem. Soc. Rev.* 44(3) (2015) 729-41.
- [20] H. Xue, J. Zhao, Q. Zhou, D. Pan, Y. Zhang, Y. Zhang, Y. Shen, Boosting the Sensitivity of a Photoelectrochemical Immunoassay by Using SiO₂@polydopamine Core-Shell Nanoparticles as a Highly Efficient Quencher, *ACS Appl. Nano Mater.* 2(3) (2019) 1579-1588.
- [21] I. Willner, F. Patolsky, J. Wasserman, Photoelectrochemistry with controlled DNA-cross-linked CdS nanoparticle arrays, *Angew. Chem. Int. Ed.* 40(10) (2001) 1861-1864.
- [22] M. Amouzadeh Tabrizi, M. Shamsipur, R. Saber, S. Sarkar, V. Ebrahimi, A high sensitive visible light-driven photoelectrochemical aptasensor for shrimp allergen

tropomyosin detection using graphitic carbon nitride-TiO₂ nanocomposite, *Biosens. Bioelectron.* 98 (2017) 113-118.

[23] P.P. Li, Y. Cao, C.J. Mao, B.K. Jin, J.J. Zhu, TiO₂/g-C₃N₄/CdS Nanocomposite-Based Photoelectrochemical Biosensor for Ultrasensitive Evaluation of T4 Polynucleotide Kinase Activity, *Anal. Chem.* 91(2) (2019) 1563-1570.

[24] W. Li, P. Sheng, J. Cai, H. Feng, Q. Cai, Highly sensitive and selective photoelectrochemical biosensor platform for polybrominated diphenyl ether detection using the quantum dots sensitized three-dimensional, macroporous ZnO nanosheet photoelectrode, *Biosens. Bioelectron.* 61 (2014) 209-14.

[25] Y. Yang, W. Hu, Bifunctional polydopamine thin film coated zinc oxide nanorods for label-free photoelectrochemical immunoassay, *Talanta* 166 (2017) 141-147.

[26] Q. Han, R. Wang, B. Xing, H. Chi, D. Wu, Q. Wei, Label-free photoelectrochemical aptasensor for tetracycline detection based on cerium doped CdS sensitized BiYWO₆, *Biosens. Bioelectron.* 106 (2018) 7-13.

[27] X. Qin, X. Zhang, M. Wang, Y. Dong, J. Liu, Z. Zhu, M. Li, D. Yang, Y. Shao, Fabrication of Tris(bipyridine)ruthenium(II)-Functionalized Metal-Organic Framework Thin Films by Electrochemically Assisted Self-Assembly Technique for Electrochemiluminescent Immunoassay, *Anal. Chem.* 90(19) (2018) 11622-11628.

[28] Q. Zhou, H. Xue, Y. Zhang, Y. Lv, H. Li, S. Liu, Y. Shen, Y. Zhang, Metal-Free All-Carbon Nanohybrid for Ultrasensitive Photoelectrochemical Immunosensing of alpha-Fetoprotein, *ACS Sens.* 3(7) (2018) 1385-1391.

[29] Y. Tan, M. Li, X. Ye, Z. Wang, Y. Wang, C. Li, Ionic liquid auxiliary exfoliation of WS₂ nanosheets and the enhanced effect of hollow gold nanospheres on their photoelectrochemical sensing towards human epididymis protein 4, *Sens. Actuators B* 262 (2018) 982-990.

[30] J. Li, L. Jiang, S. Chen, A. Kirchon, B. Li, Y. Li, H.C. Zhou, Metal-Organic Framework Containing Planar Metal-Binding Sites: Efficiently and Cost-Effectively Enhancing the Kinetic Separation of C₂H₂/C₂H₄, *J. Am. Chem. Soc.* 141(9) (2019) 3807-3811.

- [31] L. Jiao, J.Y.R. Seow, W.S. Skinner, Z.U. Wang, H.-L. Jiang, Metal–organic frameworks: Structures and functional applications, *Mater. Today* 27 (2019) 43-68.
- [32] H. Wu, Q. Gong, D.H. Olson, J. Li, Commensurate adsorption of hydrocarbons and alcohols in microporous metal organic frameworks, *Chem. Rev.* 112(2) (2012) 836-68.
- [33] H. Li, M. Eddaoudi, M. O’Keeffe, O.M. Yaghi, Design and synthesis of an exceptionally stable and highly porous metal-organic framework, *Nature* 402(6759) (1999) 276-279.
- [34] Z. Wang, Z. Yan, F. Wang, J. Cai, L. Guo, J. Su, Y. Liu, Highly sensitive photoelectrochemical biosensor for kinase activity detection and inhibition based on the surface defect recognition and multiple signal amplification of metal-organic frameworks, *Biosens. Bioelectron.* 97 (2017) 107-114.
- [35] T. Wu, T. Yan, X. Zhang, Y. Feng, D. Wei, M. Sun, B. Du, Q. Wei, A competitive photoelectrochemical immunosensor for the detection of diethylstilbestrol based on an Au/UiO-66(NH₂)/CdS matrix and a direct Z-scheme Melem/CdTe heterojunction as labels, *Biosens. Bioelectron.* 117 (2018) 575-582.
- [36] Q. Wei, C. Wang, X. Zhou, T. Wu, Y. Wang, C. Li, N. Yang, Ionic liquid and spatially confined gold nanoparticles enhanced photoelectrochemical response of zinc-metal organic frameworks and immunosensing squamous cell carcinoma antigen, *Biosens. Bioelectron.* 142 (2019) 111540.
- [37] G.Y. Zhang, Y.H. Zhuang, D. Shan, G.F. Su, S. Cosnier, X.J. Zhang, Zirconium-Based Porphyrinic Metal-Organic Framework (PCN-222): Enhanced Photoelectrochemical Response and Its Application for Label-Free Phosphoprotein Detection, *Anal. Chem.* 88(22) (2016) 11207-11212.
- [38] Y. Wang, H. Yin, X. Li, G.I.N. Waterhouse, S. Ai, Photoelectrochemical immunosensor for N⁶-methyladenine detection based on Ru@UiO-66, Bi₂O₃ and Black TiO₂, *Biosens. Bioelectron.* 131 (2019) 163-170.
- [39] G. Zhang, D. Shan, H. Dong, S. Cosnier, K.A. Al-Ghanim, Z. Ahmad, S. Mahboob, X. Zhang, DNA-Mediated Nanoscale Metal-Organic Frameworks for

Ultrasensitive Photoelectrochemical Enzyme-Free Immunoassay, *Anal. Chem.* 90(20) (2018) 12284-12291.

[40] D. Pan, G. Li, H. Hu, H. Xue, M. Zhang, M. Zhu, X. Gong, Y. Zhang, Y. Wan, Y. Shen, Direct Immunoassay for Facile and Sensitive Detection of Small Molecule Aflatoxin B₁ based on Nanobody, *Chem.Eur.J.* 24(39) (2018) 9869-9876.

[41] X. Ren, J.R. Yan, D. Wu, Q. Wei, Y.K. Wan, Nanobody-Based Apolipoprotein E Immunosensor for Point-of-Care Testing, *ACS Sens.* 2(9) (2017) 1267-1271.

[42] H. Liu, S. Xu, Z. He, A. Deng, J.J. Zhu, Supersandwich cytosensor for selective and ultrasensitive detection of cancer cells using aptamer-DNA concatamer-quantum dots probes, *Anal. Chem.* 85(6) (2013) 3385-92.

[43] J. Park, Q. Jiang, D. Feng, L. Mao, H.C. Zhou, Size-Controlled Synthesis of Porphyrinic Metal-Organic Framework and Functionalization for Targeted Photodynamic Therapy, *J. Am. Chem. Soc.* 138(10) (2016) 3518-25.

[44] Y. Zhang, D. Pan, Q. Zhou, J. Zhao, N. Pan, Y. Zhang, L.-x. Wang, Y. Shen, An enzyme cascade-based electrochemical immunoassay using a polydopamine-carbon nanotube nanocomposite for signal amplification, *J. Mater. Chem. B* 6(48) (2018) 8180-8187.

[45] H. Lee, S.M. Dellatore, W.M. Miller, P.B. Messersmith, Mussel-inspired surface chemistry for multifunctional coatings, *Science* 318(5849) (2007) 426-430.

[46] H.J. Son, S.Y. Jin, S. Patwardhan, S.J. Wezenberg, N.C. Jeong, M. So, C.E. Wilmer, A.A. Sarjeant, G.C. Schatz, R.Q. Snurr, O.K. Farha, G.P. Wiederrecht, J.T. Hupp, Light-Harvesting and Ultrafast Energy Migration in Porphyrin-Based Metal-Organic Frameworks, *J. Am. Chem. Soc.* 135(2) (2013) 862-869.

[47] A. Yella, H.W. Lee, H.N. Tsao, C.Y. Yi, A.K. Chandiran, Porphyrin-sensitized solar cells with cobalt (II/III)-based redox electrolyte exceed 12 percent efficiency (vol 334, pg 629, 2011), *Science* 334(6060) (2011) 1203-1203.

[48] W.Y. Gao, M. Chrzanowski, S.Q. Ma, Metal-metalloporphyrin frameworks: a resurging class of functional materials, *Chem. Soc. Rev.* 43(16) (2014) 5841-5866.

[49] R.W. Larsen, J. Miksovská, R.L. Musselman, L. Wojtas, Ground- and

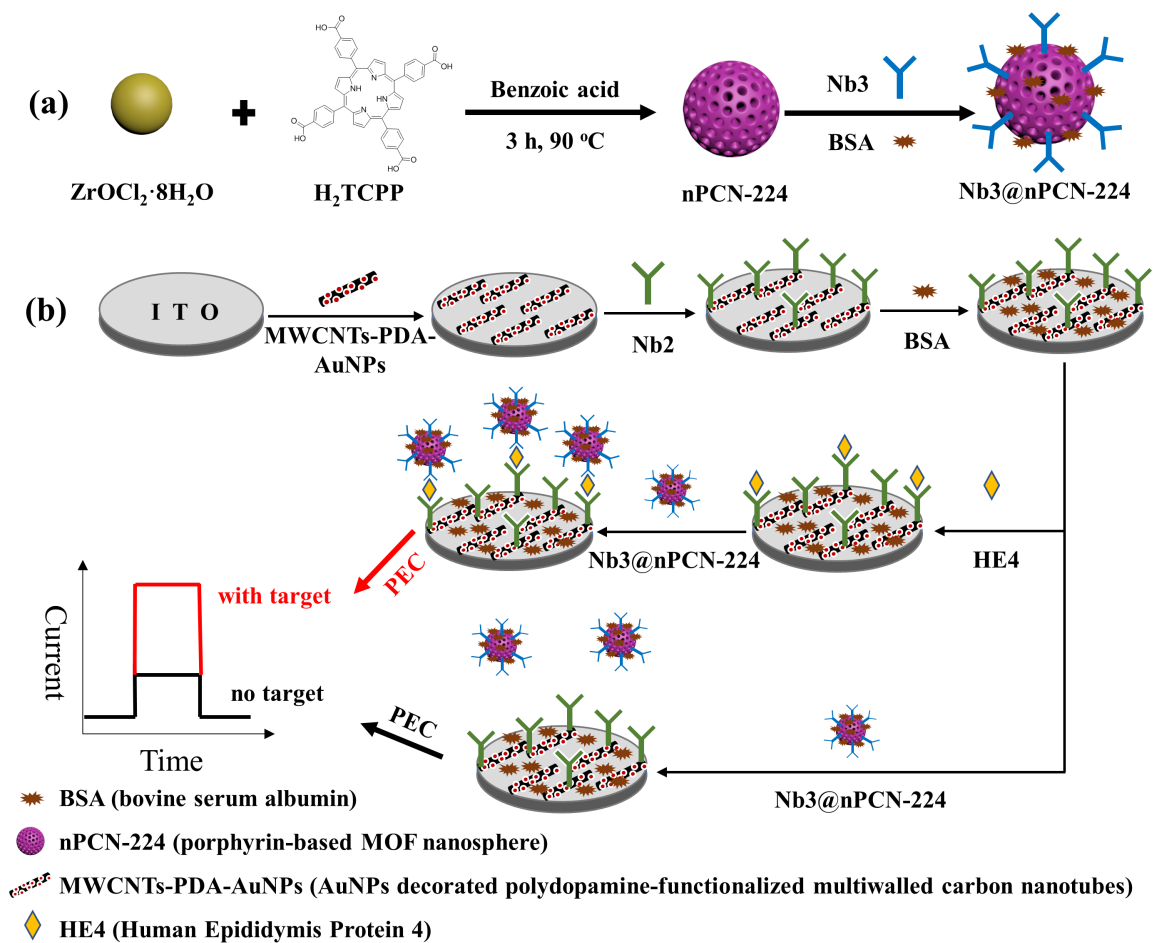
excited-state properties of Zn(II) tetrakis(4-tetramethylpyridyl) porphyrin specifically encapsulated within a Zn(II) HKUST metal-organic framework, *J. Phys. Chem. A* 115(42) (2011) 11519-24.

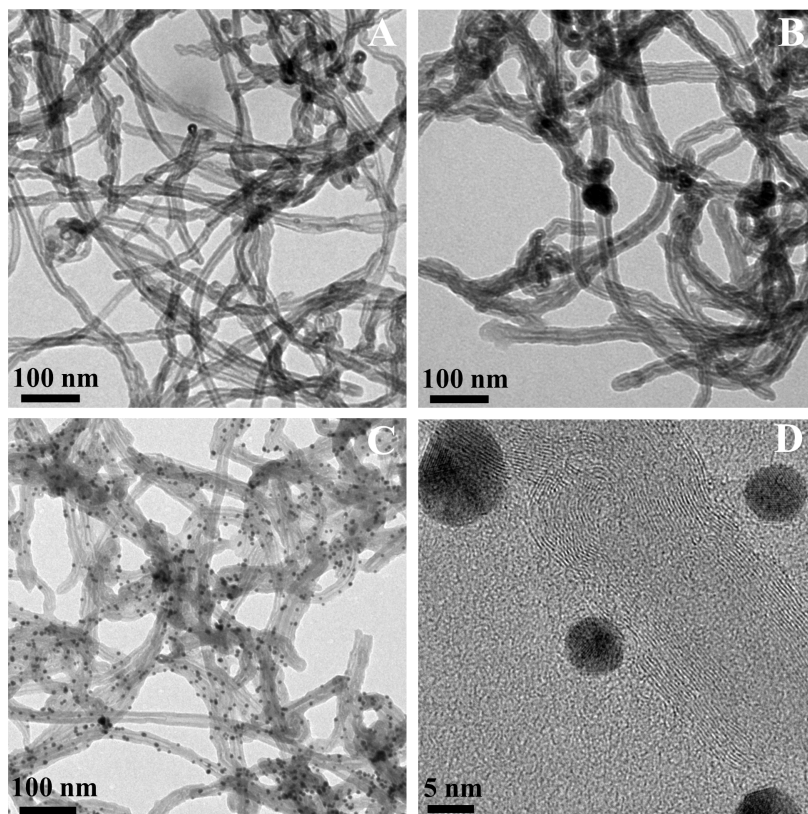
[50] H. Wang, S.L. Jiang, S.C. Chen, D.D. Li, X.D. Zhang, W. Shao, X.S. Sun, J.F. Xie, Z. Zhao, Q. Zhang, Y.P. Tian, Y. Xie, Enhanced Singlet Oxygen Generation in Oxidized Graphitic Carbon Nitride for Organic Synthesis, *Adv. Mater.* 28(32) (2016) 6940-+.

[51] F. He, L. Mi, Y.F. Shen, T. Mori, S.Q. Liu, Y.J. Zhang, Fe-N-C Artificial Enzyme: Activation of Oxygen for Dehydrogenation and Monoxygenation of Organic Substrates under Mild Condition and Cancer Therapeutic Application, *ACS Appl. Mater. Interfaces* 10(41) (2018) 35327-35333.

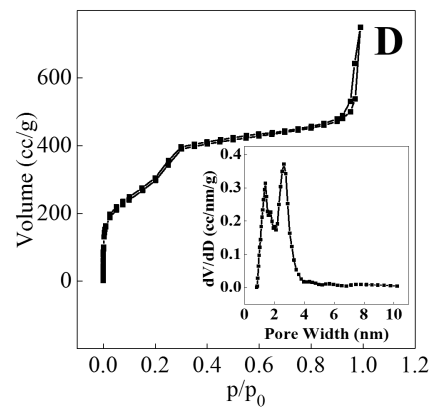
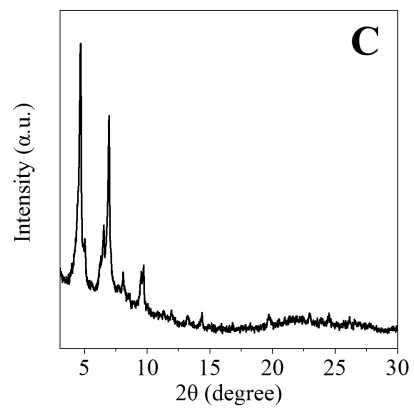
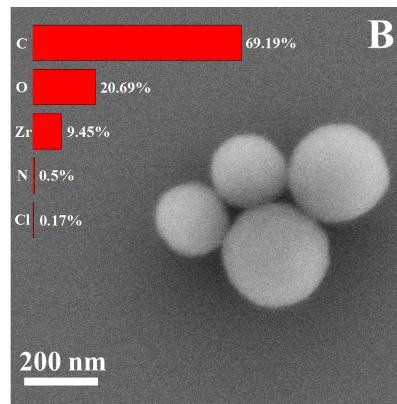
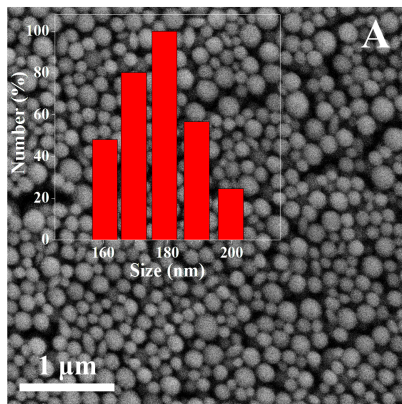
[52] T. Granato, M.G. Porpora, F. Longo, A. Angeloni, L. Manganaro, E. Anastasi, HE4 in the differential diagnosis of ovarian masses, *Clin. Chim. Acta* 446 (2015) 147-55.

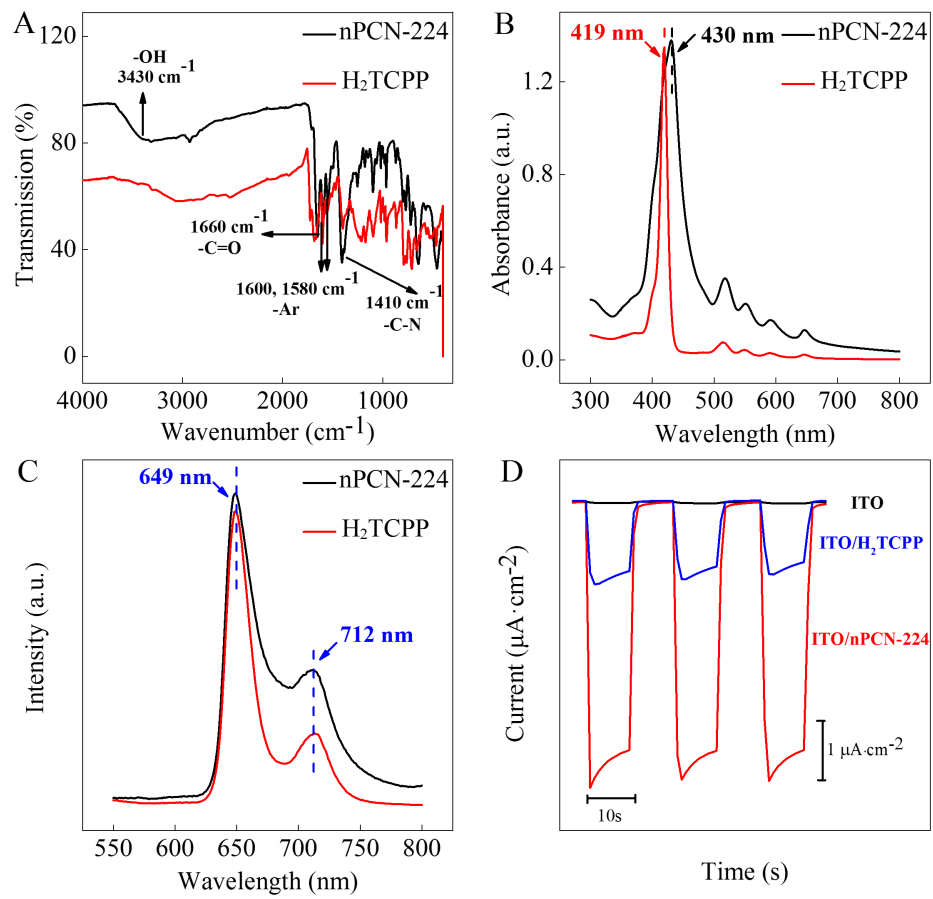
[53] D.D. Fang, M.A. Pan, H. Yi, H. Dai, Z.S. Hong, X.Q. Zheng, Y.Y. Lin, Enhanced electrochemiluminescence of luminol-DBAE system based on self-assembled mesocrystalline hybrid for the detection of ovarian cancer marker, *Sens. Actuators B* 286 (2019) 608-615.

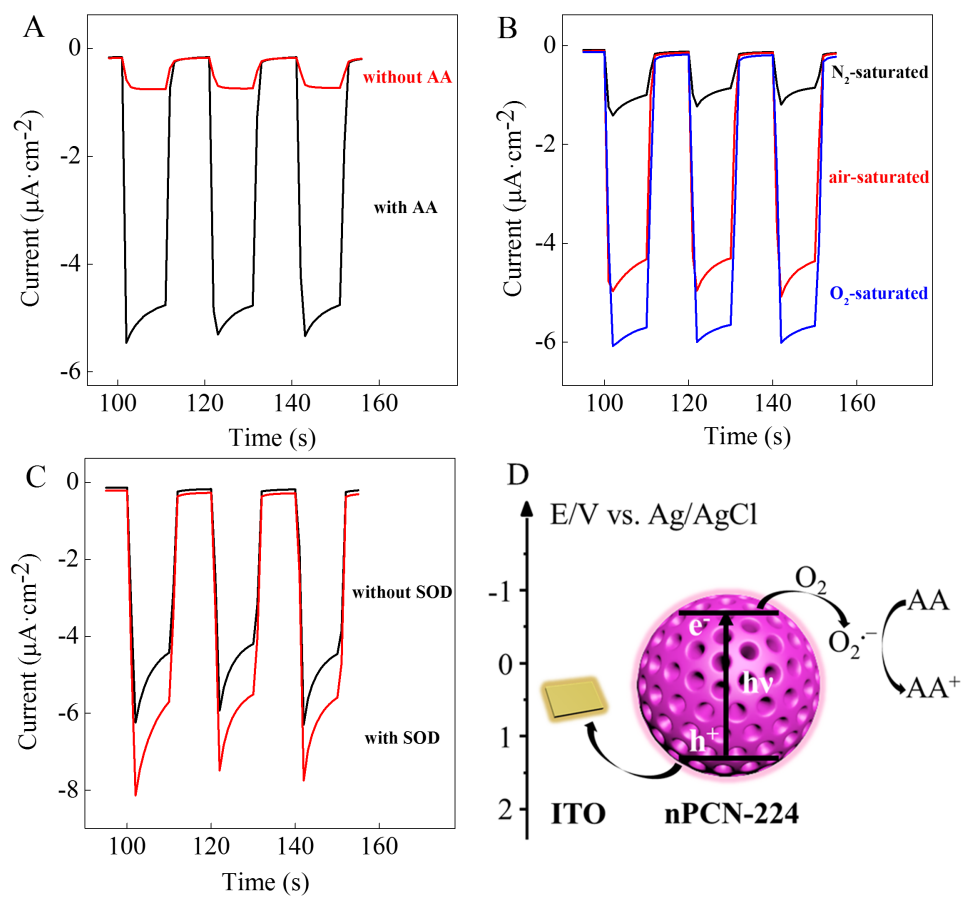


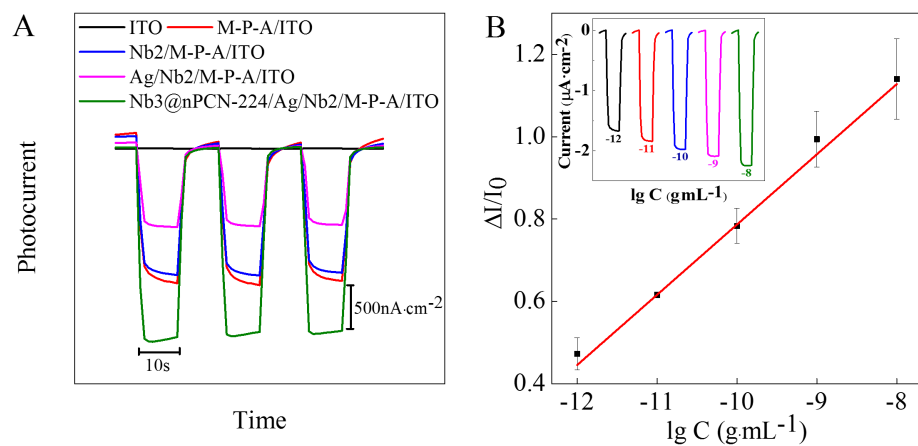


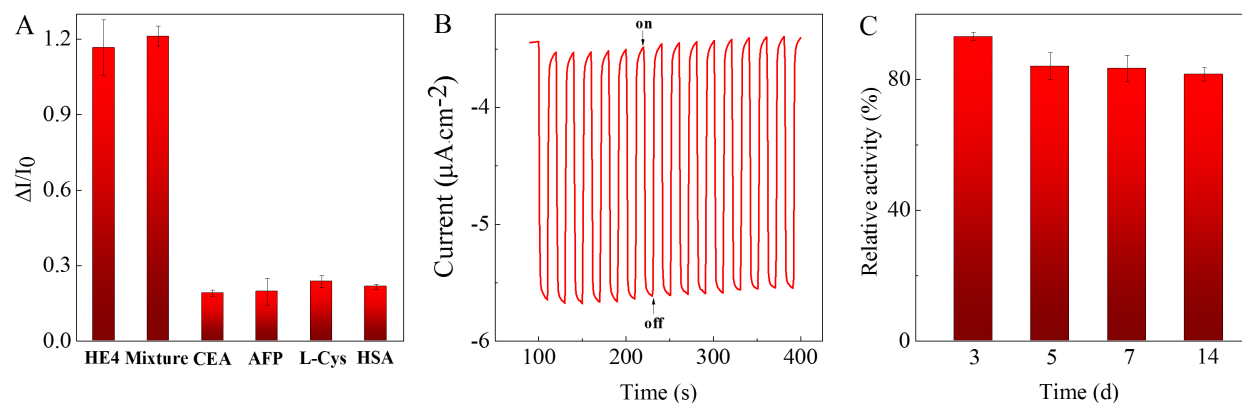
Journal

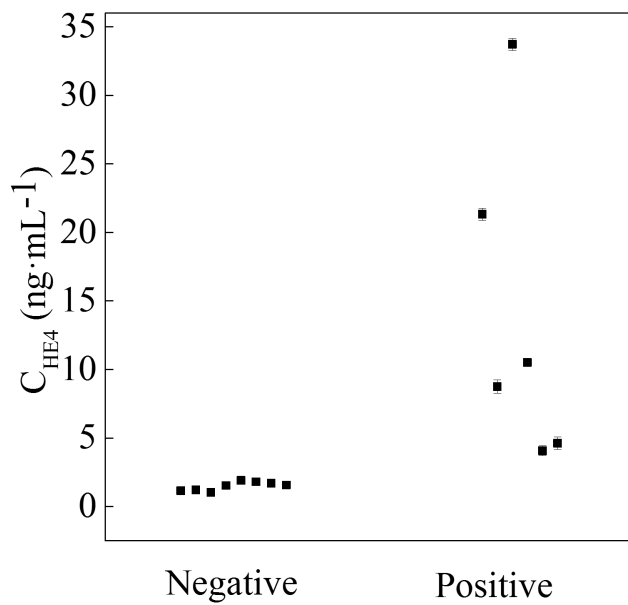












Journal

Highlights:

- A “signal on” immunosensor for HE4 was constructed using MOF nanospheres as PEC probes.
- The MOF with high porosity guaranteed the enrichment of O₂ and AA, promoting charge separation.
- Nanobodies were used instead of monoclonal antibody considering the small size of HE4.
- The sensor can distinguish ovarian cancer patients in different stages from healthy individuals.

Declaration of interests

The authors declare that they have no known competing financial interests or personal relationships that could have appeared to influence the work reported in this paper.

The authors declare the following financial interests/personal relationships which may be considered as potential competing interests:

Journal Pre-proof